IEEE Photonics Journal
An IEEE Photonics Society Publication

Open Access

# Analysis and Design Optimization of a Hybrid $VO_2$/Silicon $2 \times 2$ Microring Switch

Volume 8, Number 2, April 2016

L. Sanchez
S. Lechago
A. Gutierrez
P. Sanchis

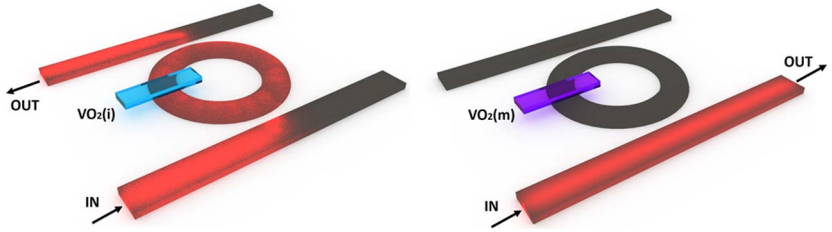


DOI: 10.1109/JPHOT.2016.2551463
1943-0655 

IEEE photonics SOCIETY
IEEE

# Analysis and Design Optimization of a Hybrid $VO_2$/Silicon $2 \times 2$ Microring Switch

**L. Sanchez, S. Lechago, A. Gutierrez, and P. Sanchis**

Nanophotonics Technology Center, Universitat Politecnica de Valencia, 46022 Valencia, Spain

*DOI: 10.1109/JPHOT.2016.2551463*


Manuscript received March 11, 2016; accepted March 26, 2016. Date of publication April 6, 2016; date of current version April 20, 2016. This work was supported by the European Commission under Project FP7-ICT-2013-11-619456 SITOGA. This work was also supported by LEOMIS (TEC2012-38540) and NANOMET PLUS-Conselleria d'Educació, Cultura i Esport (PROMETEOII/2014/034). The work of L. Sánchez was supported by the Generalitat Valenciana in the context of the VALi+d program. Corresponding author: P. Sanchis (e-mail: pabsanki@ntc.upv.es).

**Abstract:** The metal-to-insulator transition (MIT) property of vanadium dioxide ($VO_2$) has recently been used in several application fields such as plasmonics, sensing, metamaterials, and optical modulation. Due to the MIT nature, $VO_2$ allows a huge change in its complex refractive index that can be electrooptically controlled. In this paper, the analysis and design optimization of a $2 \times 2$ microring switch based on a hybrid $VO_2$/silicon waveguide structure is addressed. Switching is achieved by exploiting the change in both absorption loss and phase shift that occurs in $VO_2$ when changing from the insulating to the metallic state. The device is optimized to minimize insertion losses and crosstalk. An active length of only 2.8 $\mu$m is required to achieve a data throughput rate higher than 500 Gb/s at a single optical wavelength.

**Index Terms:** Integrated optical devices, silicon photonics, optical switches and phase change materials.

## 1. Introduction

The microring resonator is a very versatile photonic component that has been proposed for enabling a large variety of passive and active functionalities such as (de)multiplexing, filtering, modulating, switching, or sensing [1]. Ultra-small footprint and low power consumption are usual requirements for the integration of active devices in photonic integrated circuits and, in particular, they play a key role in electro-optical switches designs. To this end, the combination of high-contrast waveguides and active materials together with microring resonator structures provides a unique path towards the development of switching components with best performance. Active materials allow tuning their optical properties as function of an external stimulus. Amongst them, vanadium dioxide ($VO_2$) has been largely investigated for different applications due to its controllable change between an insulator and a metallic phase [2]. For photonic applications, $VO_2$ shows a promising performance due to the abrupt change in the refractive index between the two phases in the metal-to-insulator transition (MIT). The complex refractive index changes from $3.21 + 0.17i$ in the insulating phase to about $2.15 + 2.79i$ in the metallic phase at $\lambda = 1550$ nm [3]. At steady conditions, $VO_2$ is in the insulator state (high transparence

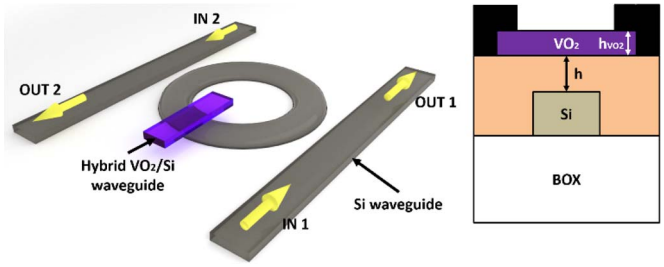


Fig. 1. (a) Concept art of the 2 × 2 switch based on an add–drop microring resonator. (b) Schematic of the hybrid waveguide. The electrodes are represented in black.

in the infrared spectrum), but its phase can be triggered to a metallic state (absorbing properties) by applying an electric field [4]–[8], optical pumping [9], [10], or heating [11], [12]. The huge change in the refractive index can give rise to a significant reduction in power consumption, as well as in active length. Therefore, $VO_2$ has been proposed for the development of ultra-compact modulators and switches in the silicon photonics platform. So far all the structures have been based on a one input/one output (1 × 1) configuration. Optical switches based on ring resonator structures have been proposed to exploit the change in the real part of the $VO_2$ refractive index [9] and extinction ratios up to 10 dB have been experimentally reported [10]. On the other hand, the change in the imaginary part of the $VO_2$ refractive index has been used for enabling electro-absorption modulators. Hybrid structures based on the silicon waveguide covered with a $VO_2$ patch ranging from 0.5 $\mu$m to 1 $\mu$m have been demonstrated showing modulation depths of 4 dB/$\mu$m and insertion losses between 0.5 dB to 2 dB [9]. More recently, a 1 $\mu$m long electro-absorption switch with an extinction ratio higher than 10 dB and modest insertion losses of 5 dB has been demonstrated [13]. The integration of the $VO_2$ into plasmonics structures has also been proposed [14]–[19]. Electrically driven $VO_2$ plasmonic switches with extinction ratios and insertion losses per length of 1.9 dB/$\mu$m and 0.9 dB/$\mu$m respectively have been experimentally demonstrated [18]. However, the coupling to conventional silicon waveguides is usually more challenging. A plasmonic structure with optimum coupling has been recently proposed and analyzed by means of simulations but the achieved extinction ratios were below 9 dB [19].

In this paper, the analysis and design optimization of a 2 × 2 microring switch based on a hybrid $VO_2$/silicon waveguide structure is reported for the first time. Active performance is based on the MIT in the $VO_2$ so that a change in optical absorption losses and phase shift is achieved due to the complex nature of the refractive index. Different from previous works, switching is achieved by exploiting the change in absorption loss but taking advantage of the induced phase shift to enhance the performance as well. Thus, insertion losses below 1.8 dB and crosstalk values above 12 dB are achieved in a compact switching device with an active length as low as 2.8 $\mu$m and a footprint below 100 $\mu m^2$.

## 2. Analysis of the 2 × 2 Optical Switch Structure

Fig. 1 shows the proposed 2 × 2 switch based on a conventional add-drop microring resonator structure and the schematic of the hybrid $VO_2$/Si waveguide structure. The external waveguides are based on silicon while the ring is based on a hybrid $VO_2$/Si waveguide. The $VO_2$ is only deposited over a part of the ring. A symmetric structure is required to have the same switching performance independently of the input port so the transmission coefficient of the ring will be the same at both coupling sections.

The device will switch between the bar and cross states by exploiting the change of the $VO_2$ complex refractive index. In the cross state, shown in Fig. 2(a), low losses inside the ring are

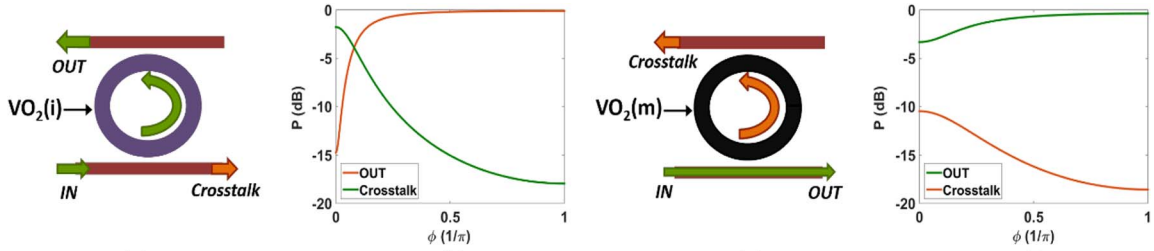


(a) (b) (c) (d)

Fig. 2. Switch operation in (a) the cross state and (c) the bar state. Transmission response as a function of the phase shift taking into account $t = 0.88$ and losses in the ring of (b) 0.5 dB and (d) 5 dB.

required to minimize the insertion loss of the switch. Therefore, the $VO_2$ is in the insulating state. The normalized power at the output port and the crosstalk can be calculated by

$$P_{\text{out}} = \frac{a_i(1-t^2)^2}{1-2t^2a_i\cos\phi_i + (t^2a_i)^2} \tag{1}$$

$$P_{\text{crosstalk}} = \frac{t^2a_i^2 - 2t^2a_i\cos\phi_i + t^2}{1-2t^2a_i\cos\phi_i + (t^2a_i)^2} \tag{2}$$

where $t$ is the transmission coefficient, $\emptyset_i$ is the phase shift and $a_i$ is the amplitude losses in the ring for the insulating state [1]. Fig. 2(b) shows the normalized output power and crosstalk for a value of $A_i = 20\log_{10}(a_i) = 0.5$ dB and a transmission coefficient of 0.88. It can be seen that the lowest insertion losses and highest crosstalk are obtained by placing the input optical signal at the ring resonance $(\emptyset_i = 0)$.

On the other hand, in the bar state, shown in Fig. 2(c), the $VO_2$ will change to the metallic state. Therefore, losses in the ring will increase to $a_m$ due to the variation of the imaginary part of the refractive index. In this case, the output power of the switch is calculated by (2) and the crosstalk by (1) taking into account the new ring loss value of $a_m$. Low insertion losses and high crosstalk can also be achieved as it can be seen in Fig. 2(d), which depicts the switching performance for a value of $A_m = 20\log_{10}(a_m) = 5$ dB and the same transmission coefficient as in Fig. 2(b). It should be noticed that the change in the real part of the $VO_2$ refractive index will give rise to a phase shift difference with respect to the insulating state $(\emptyset_m > \emptyset_i)$ that will contribute to improve the insertion losses and crosstalk in the switch, as it can be seen in Fig. 2(d). The same insertion losses are desirable for both switching states which can be achieved by conveniently designing the transmission coefficient of the ring structure. Fig. 3 shows the insertion losses and crosstalk as a function of the transmission coefficient for the same cross ($\emptyset_i = 0$, $A_i = 0.5$ dB) and bar ($\emptyset_m = 0.2\pi$, $A_m = 5$ dB) states considered in Fig. 2(b) and (d), respectively. It can be seen that there is a transmission coefficient value, $t = 0.88$ in Fig. 3(a), that allows obtaining the same insertion losses at both switching states although the crosstalk level is slightly different. It is interesting to notice that there is also a different transmission coefficient that provides the same crosstalk level, as it can be seen in Fig. 3(b).

Switching can be achieved by only varying the losses in the ring. Fig. 4 shows the insertion losses and transmission coefficient depending on the loss difference $(\Delta\alpha = A_m - A_i)$ between the bar and cross states by assuming that the phase shift is zero $(\Delta\emptyset = \emptyset_m - \emptyset_i = 0)$. It can be seen that low insertion losses can be achieved by only varying the ring losses between the two switching states. However, there is a bound in the lowest insertion loss that is determined by the ring loss in the cross state $(A_i)$. Insertion losses below 1.5 dB can be achieved if the ring loss in the cross state is 0.5 dB, which is possible to achieve with the value of the $VO_2$ refractive index in the insulating state. Lower insertion losses can be achieved by reducing the ring loss at the cross state but then a higher transmission coefficient will be required that

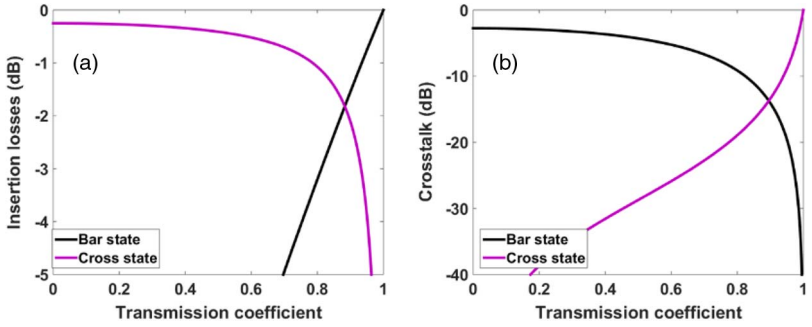


Fig. 3. (a) Insertion losses and (b) crosstalk level as function of the transmission coefficient taking into account $\emptyset_i = 0$ and $A_i = 0.5$ dB for the cross state and $\emptyset_m = 0.2\pi$ and $A_m = 5$ dB for the bar state.

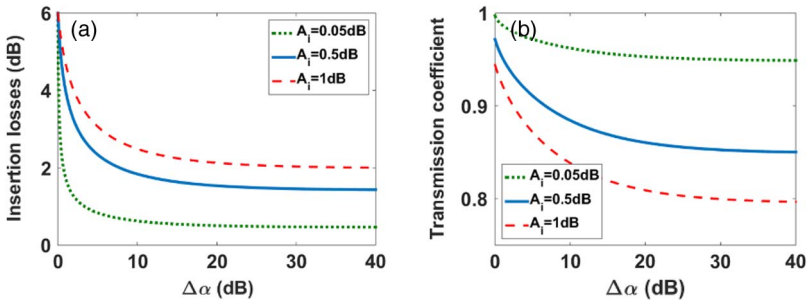


Fig. 4. (a) Insertion losses and (b) transmission coefficient as a function of the ring loss difference $(\Delta\alpha)$ between the bar and cross states by assuming that the phase-shift variation is zero $(\Delta\emptyset = 0)$.

will decrease the bandwidth of the ring resonance and, therefore, the optical bandwidth of the switch.

Fig. 5 shows the switching performance as a function of the ring loss difference between the bar and cross states by considering that the ring loss in the cross state is 0.5 dB. Furthermore, the impact of having an additional phase shift is also depicted. It can be seen that if the loss difference is large enough $(\Delta\alpha > 20$ dB$)$, low insertion losses and high crosstalk at both switching states are achieved without requiring any phase shift and for a transmission coefficient around 0.85. In fact, the influence of the phase shift in the switching performance is negligible. However, a good performance can also be achieved with a lower loss difference if there is a certain phase shift, for instance $\Delta\emptyset = 0.25\pi$ as it is shown in Fig. 5. Insertion losses below 1 dB are only achieved by having a $\pi$-phase shift and keeping the loss difference below 7 dB. In this case, it should be noticed that a negligible loss difference is not desired as then crosstalk will increase at the bar state.

Therefore, the optimum hybrid $VO_2$/Si waveguide will be designed by exploiting both the loss difference and phase shift variation between the insulating and metallic states. On the other hand, the active length will be determined to ensure that losses in the insulating state are 0.5 dB.

## 3. Hybrid $VO_2$/Si Waveguide Design

A standard silicon waveguide $(n_{Si} = 3.475)$ with a cross section of 480 $\times$ 220 nm is considered. The waveguide is covered by a silica cladding $(n_{SiO2} = 1.444)$ that is etched down and planarized close to the waveguide. The $VO_2$ film is then deposited and metal contacts are placed on both sides of the waveguide. The optimum spacer, $h$, and $VO_2$ film thickness, $h_{VO2}$, have been designed to achieve the best performance in terms of insertion losses and crosstalk. The design has been carried out with a commercial mode solver based on the finite element method. The

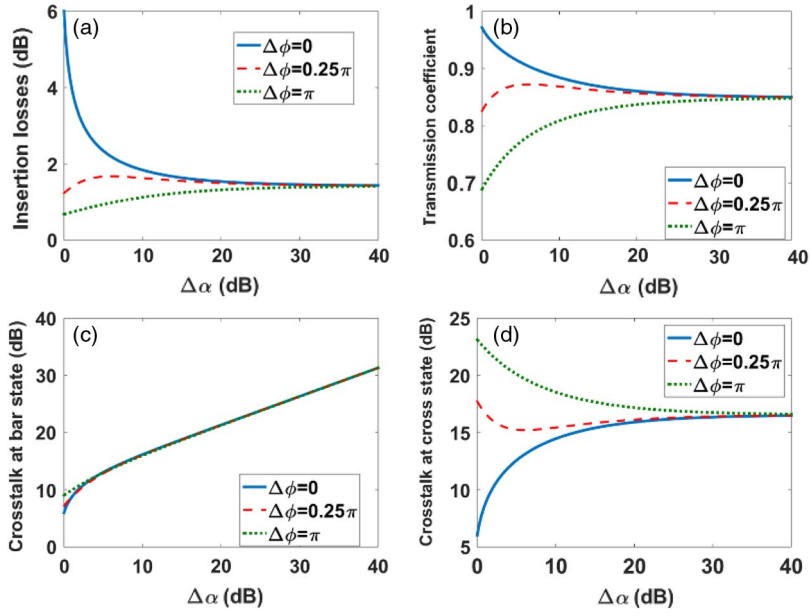


Fig. 5. (a) Insertion losses, (b) transmission coefficient, (c) crosstalk at the bar state, and (d) crosstalk at the cross state as a function of the ring loss difference between the two switching states. The ring loss in the cross state is $A_i = 0.5$ dB.

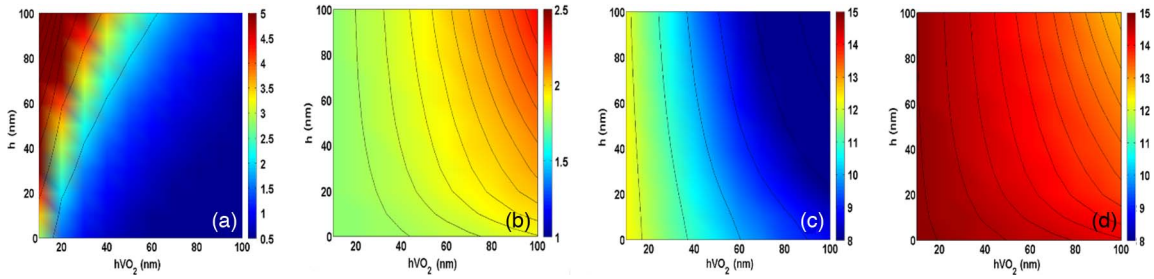


Fig. 6. (a) Active length, (b) insertion loss, and crosstalk at (c) the bar state and (d) the cross state for TE polarization.

active length, insertion loss, and crosstalk at the bar and cross states as a function of $h$ and $h_{VO2}$ parameters is shown in Fig. 6 for TE polarization. It can be seen that both insertion losses and crosstalk are maximized as the $VO_2$ layer is thinner while the influence of varying the spacer thickness is low. However, the active length is minimized for thinner spacers. Therefore, lower spacer and $VO_2$ thicknesses are desirable to achieve the optimum switching performance. For a 10 nm-thick $VO_2$ film deposited on top of the silicon waveguide $(h = 0$ nm$)$, an active length of 2.8 $\mu$m will be required to ensure insertion losses of 1.75 dB and a crosstalk higher than 12 dB at both switching states.

Results for TM polarization are shown in Fig. 7. In this case, it can be seen that there is a region where low insertion losses are achieved. Insertion losses as low as 1.3 dB are possible but the crosstalk at bar state will be below 10 dB. Therefore, there is a trade-off between the insertion losses and crosstalk levels at both states. For a $VO_2$ film with a thickness of 40 nm and a spacer of 20 nm, crosstalk levels higher than 16 dB and insertion losses of 1.5 dB are achieved by using an ultra-short active length of only 0.62 $\mu$m.

Fig. 8 shows the different mode profiles as function of the polarization and the $VO_2$ state for the waveguide structure with the optimum parameters previously designed. For TE polarization, the mode does not experiment a huge change in its mode profile when the $VO_2$ changes from

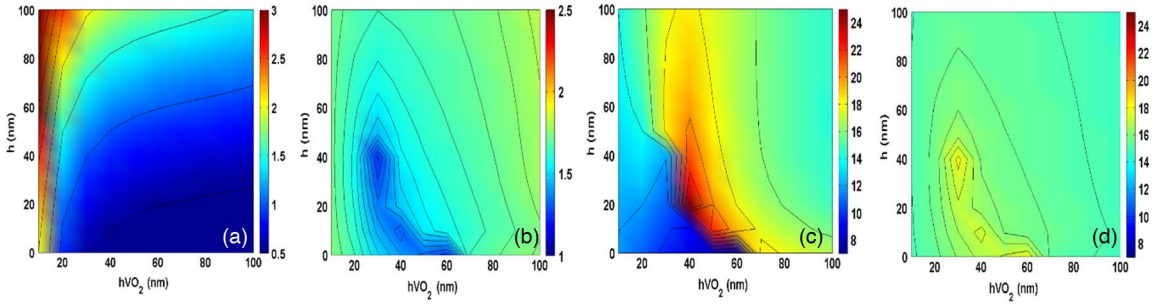


Fig. 7. (a) Active length, (b) insertion loss, and crosstalk at (c) the bar state and (d) the cross state for TM polarization.

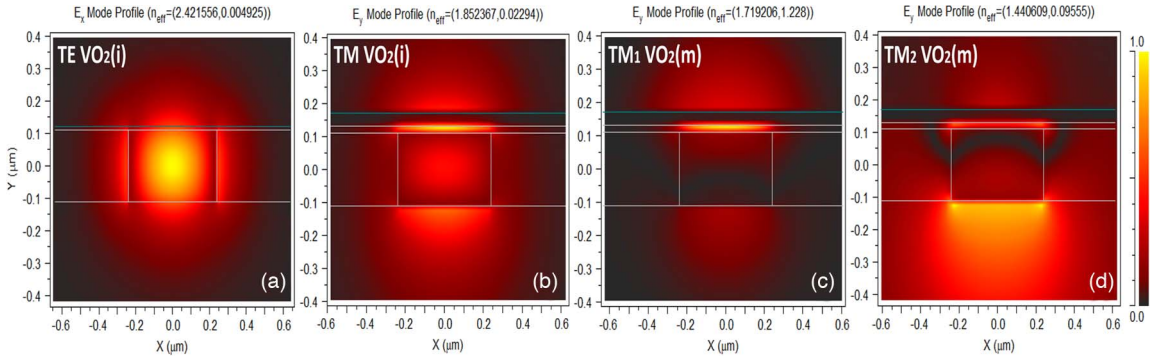


Fig. 8. For $\lambda = 1550$ nm, mode profile in the insulating state for (a) TE and (b) TM polarizations. (c) First mode and (d) second mode that appear in the metallic state for TM polarization.

the insulating state, which is shown in Fig. 8(a), to the metallic state. On the other hand, for TM polarization the mode in the insulating state is highly confined in the slot between the $VO_2$ and the waveguide, as it can be seen in Fig. 8(b). However, when the $VO_2$ switches to the metallic state, the waveguide becomes multimode and two possible modes appear. Fig. 8(c) shows the mode considered to obtain the results shown in Fig. 7. It can be seen that the mode profile is similar with respect to the insulating state but there is a large variation in the imaginary part of the effective index that gives rise to a high loss difference of 26.3 dB. However, a very small loss difference of only 1.67 dB is achieved with the second mode shown in Fig. 8(d) basically because the mode profile is significantly changed compared to the insulating state, and there is less optical confinement in the $VO_2$ layer.

The optimum hybrid $VO_2$/Si waveguides for each polarization have also been simulated by 3D-FDTD to analyze the transmission performance and coupling losses due to the modal mismatch between the silicon and hybrid $VO_2$/Si waveguides. Fig. 9 shows the electric field contour maps for both polarizations and $VO_2$ states. For TE polarization, coupling losses are negligible and the transmission performance is in excellent agreement with simulation results obtained from the modal analysis. Thereby, losses in the insulating state, shown in Fig. 9(a), are 0.5 dB while they increase to around 5 dB when the $VO_2$ changes to the metallic state, shown in Fig. 9(c). It should be reminded that the $VO_2$/Si waveguide length has been designed to have only 0.5 dB losses at the insulating state. However, for TM polarization, the total losses of the structure shown in Fig. 9(b) with $VO_2$ in the insulating state increase to 2.1 dB due to an inefficient coupling. In this case, coupling losses cannot be neglected because there is a higher mode mismatch between the TM mode in the silicon waveguide and the TM mode in the hybrid $VO_2$/Si waveguide. Furthermore, losses of only 4.8 dB have been obtained when the $VO_2$ changes to the metallic state, which is shown in Fig. 9(d). These losses are much smaller than the expected ones of around 26.8 dB due to the multimode performance of the hybrid $VO_2$/Si

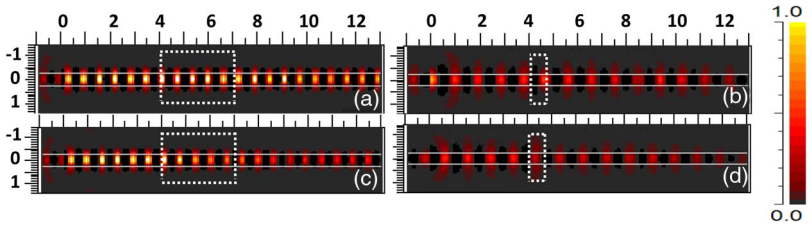


Fig. 9. Three-dimensional FDTD simulations of the designed hybrid $VO_2$/Si waveguide, which is depicted with a white dashed rectangle, in (a) the insulating state and (c) the metallic state for TE polarization and in (b) the insulating state and (d) the metallic state for TM polarization. The hybrid waveguide length is 2.8 $\mu$m for TE polarization and 0.62 $\mu$m for TM polarization.

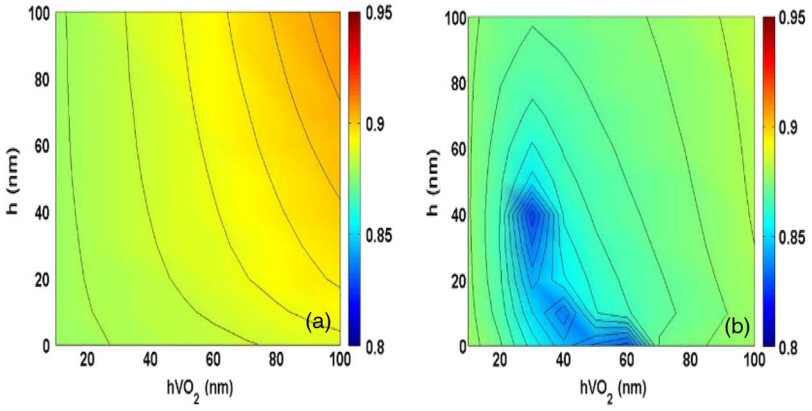


Fig. 10. Required transmission coefficient as function of h and hVO2 for (a) TE and (b) TM polarizations.

waveguide. More concretely, the undesired second TM mode, which is depicted in Fig. 8(d), is also partially excited thus contributing to reduce the total losses of the structure that will, therefore, have a negative impact on the switching performance.

## 4. $VO_2$/Si Microring Switch Performance

Fig. 10 shows the required transmission coefficient in the microring resonator to obtain the insertion losses and crosstalk results depicted in Figs. 6 and 7. According to the designed values of h and $h_{VO2}$ for each polarization, the optimum transmission coefficient is $t = 0.88$ for TE and $t = 0.85$ for TM polarizations. However, the preferred polarization for the switch is TE due to the better transmission performance and negligible coupling losses with the silicon waveguide. Furthermore, most of the photonic circuits based on silicon photonics work also with TE polarization and a smaller radius, and therefore, a more compact switching device can also be achieved due to the smaller bending losses compared to TM polarization.

Three-dimensional-FDTD simulations have been carried out to determine the required gap between the ring and the input/output waveguides to obtain the required transmission coefficient for TE polarization. A radius to the midpoint of the ring of 3.5 $\mu$m has been first chosen for a compact footprint below 100 $\mu m^2$. For such radius, a gap of 30 nm has been obtained that could be increased by using a racetrack configuration to fulfill fabrication constraints.

Three-dimensional-FDTD simulations of the final hybrid $VO_2$/Si microring switching structure have also been performed to validate the whole design. Fig. 11(a) shows the response at the cross state. In this case, the $VO_2$ is in the insulating state and the switch operates at the ring resonance. The optical bandwidth is around 3.8 nm that will allow a data throughput rate higher than 500 Gbps. Furthermore, the throughput can be increased beyond Tbps operation by using

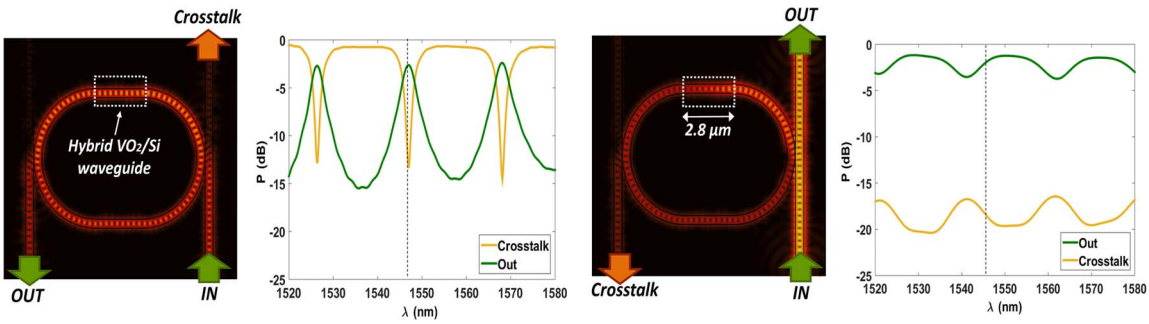


(a) (b)

Fig. 11. Three-dimensional FDTD simulations of the hybrid VO2/Si microring switch (waveguide-to-ring gap = 30 nm, $h = 0$ nm, $h_{VO2} = 10$ nm, $h_{Si} = 220$ nm, and $w_{Si} = 480$ nm) for (a) the cross state and (b) the bar state and TE input polarization. The dashed vertical line shows the operating optical wavelength.

a WDM optical signal with a wavelength spacing matched with the free spectral range of the ring resonances to simultaneously switch on and off a large number of wavelength channels [21]. Fig. 11(b) shows the response at the bar state in which the $VO_2$ is switched to the metallic state. It can be seen that the higher ring losses have a large influence on the ring resonance, which is almost suppressed. Furthermore, the resonance wavelengths are also shifted due to the additional phase shift induced by the variation in the $VO_2$ state. Both effects will contribute to improve insertion losses and reduce the crosstalk, as it can be clearly seen in Fig. 13(b) and in agreement with theoretical results depicted in Fig. 2(d).

## 5. Conclusion

The analysis and design optimization of a 2 × 2 optical switch based on a hybrid $VO_2$/Si microring structure has been carried out for both TE and TM polarizations. Extremely short active lengths have been demonstrated thus yielding to compact footprints lower than 100 $\mu m^2$. The best performance has been achieved for TE polarization. Insertion losses below 1.8 dB and crosstalk values above 12 dB have been achieved. Insertion losses can be lowered if the imaginary part of the $VO_2$ refractive index at the insulating state could be decreased. However, it should be noticed that in this case a higher transmission coefficient would also be required that would reduce the optical bandwidth of the switch. In the proposed device, the data throughput rate at a single optical wavelength will be higher than 500 Gbps, thus proving $VO_2$/Si technology as a promising approach for the development of switches with high throughput bandwidth, low power consumption, small footprint, and compatibility with silicon CMOS photonics.

## References

[1] W. Bogaerts *et al.,* "Silicon microring resonators," *Laser Photon. Rev.*, vol. 6, no. 1, pp. 47–73, Jan. 2012.
[2] A. L. Pergament, G. B. Stefanovich, and A. Velichko, "Oxide electronics and vanadium dioxide perspective: A review," *J. Sel. Topics Nano Electron. Comput.*, vol. 1, no. 1, pp. 24–43, 2013.
[3] R. M. Briggs, I. M. Pryce, and H. A. Atwater, "Compact silicon photonic waveguide modulator based on the vanadium dioxide metal-insulator phase transition," *Opt. Exp.*, vol. 18, no. 11, pp. 11192–11201, May 2010.
[4] D. Ruzmetov, G. Gopalakrishnan, J. Deng, V. Narayanamurti, and S. Ramanathan, "Electrical triggering of metal-insulator transition in nanoscale vanadium oxide junctions," *J. Appl. Phys.*, vol. 106, no. 8, 2009, Art. no. 083702.
[5] S. B. Lee, K. Kim, J. S. Oh, B. Kahng, and J. S. Lee, "Origin of variation in switching voltages in threshold-switching phenomena of $VO_2$ thin films," *Appl. Phys. Lett.*, vol. 102, no. 6, 2013, Art. no. 063501.
[6] B. G. Chae, H. T. Kim, D. H. Youn, and K. Y. Kang, "Abrupt metal-insulator transition observed in $VO_2$ thin films induced by a switching voltage pulse," *Phys. B Condens. Matter*, vol. 369, no. 1–4, pp. 76–80, 2005.
[7] A. Joushaghani *et al.,* "Voltage-controlled switching and thermal effects in $VO_2$ nano-gap junctions," *Appl. Phys. Lett.*, vol. 104, no. 22, 2014, Art. no. 221904.
[8] P. Markov *et al.,* "Optically monitored electrical switching in $VO_2$," *ACS Photon.*, vol. 2, no. 8, pp. 1175–1182, 2015.

[9] J. D. Ryckman, K. A. Hallman, R. E. Marvel, R. F. Haglund, and S. M. Weiss, "Ultra-compact silicon photonic devices reconfigured by an optically induced semiconductor-to-metal transition," *Opt. Exp.*, vol. 21, no. 9, pp. 438–446, May 2013.
[10] J. D. Ryckman *et al.,* "Photothermal optical modulation of ultra-compact hybrid Si-$VO_2$ ring resonators," *Opt. Exp.*, vol. 20, no. 12, pp. 13215–13225, 2012.
[11] A. Zimmers *et al.,* "Role of thermal heating on the voltage induced insulator-metal transition in $VO_2$," *Phys. Rev. Lett.*, vol. 110, no. 5, Feb. 2013, Art. no. 056601.
[12] M. A. Kats *et al.,* "Thermal tuning of mid-infrared plasmonic antenna arrays using a phase change material," *Opt. Lett.*, vol. 38, no. 3, pp. 368–370, 2013.
[13] A. Joushaghani *et al.,* "Wavelength-size hybrid Si-$VO_2$ waveguide electroabsorption optical switches and photodetectors," *Opt. Exp.*, vol. 23, no. 3, pp. 3657–3668, 2015.
[14] P. Markov, K. Appavoo, R. F. Haglund, and S. M. Weiss, "Hybrid Si-$VO_2$-Au optical modulator based on near-field plasmonic coupling," *Opt. Exp.*, vol. 23, no. 5, pp. 6878–6887, 2015.
[15] L. Sweatlock and K. Diest, "Vanadium dioxide based plasmonic modulators," *Opt. Exp.*, vol. 20, no. 8, pp. 8700–8709, 2012.
[16] K. J. A. Ooi, P. Bai, H. S. Chu, and L. K. Ang, "Ultracompact vanadium dioxide dual-mode plasmonic waveguide electroabsorption modulator," *Nanophotonics*, vol. 2, no. 1, pp. 13–19, 2013.
[17] J. T. Kim, "CMOS-compatible hybrid plasmonic modulator based on vanadium dioxide insulator-metal phase transition," *Opt. Lett.*, vol. 39, no. 13, pp. 3997–4000, Jul. 2014.
[18] A. Joushaghani *et al.,* "Sub-volt broadband hybrid plasmonic-vanadium dioxide switches," *Appl. Phys. Lett.*, vol. 102, no. 6, 2013, Art. no. 061101.
[19] J. Choe and J. T. Kim, "Design of vanadium dioxide-based plasmonic modulator for both TE and TM modes," *IEEE Photon. Technol. Lett.*, vol. 27, no. 5, pp. 514–517, Mar. 2015.